

Anisotropic exciton polariton pairs as a platform for PT-symmetric non-Hermitian physics

Devarshi Chakrabarty^{1†}, Avijit Dhara^{1†}, Pritam Das¹, Kritika Ghosh², Ayan Roy Chaudhuri², Sajal Dhara^{1*}

¹*Department of Physics, IIT Kharagpur, Kharagpur-721302, India*

²*Materials Science Centre, IIT Kharagpur, Kharagpur-721302, India*

[†] *These authors contributed equally*

^{*} *Corresponding author. email: sajal dhara@phy.iitkgp.ac.in*

Abstract: Non-Hermitian PT-symmetric systems can be conveniently realized in optical systems in the classical domain¹⁻⁴ and have been used to explore a plethora of exotic phenomena like loss-induced lasing^{5,6} and selective propagation of chiral modes in waveguides⁷⁻⁹. On the other hand, a microcavity exciton-polariton system is intrinsically non-Hermitian in the quantum regime¹⁰⁻¹³. However, realization of such systems in the PT-symmetric phase has not been achieved so far. Here we show how a pair of nearly orthogonal sets of anisotropic exciton-polaritons can offer a versatile platform for realizing multiple EPs¹⁴ and propose a roadmap to achieve a PT-symmetric system. By utilizing the tunability of coupling strength and energy detuning on the polarization of probe beam, the angle of incidence, and the orientation of the anisotropic sample, we realise two kinds of EPs: Polarization-tunable polariton dispersion creates one set of EPs based on tunable coupling strength, while the rotating the sample reveals Voigt EPs¹⁵ for specific orientations. Pair of anisotropic microcavity exciton-polaritons can offer a promising platform not only for fundamental research in non-Hermitian quantum physics and topological polaritons but also we have proposed that it can offer a system to realize zero threshold laser.

The exploration of non-Hermitian systems offers a window into several intriguing phenomena which are not realizable in conservative systems. The parameter space of such systems contains spectral singularities called Exceptional Points (EPs) where eigenvalues and their corresponding eigenvectors coalesce^{16–19}. The balancing of gain and loss allows a non-Hermitian system to become PT-symmetric, in which case the eigenvalues can be real. At the EPs, tuning the parameters carefully can cause a transition from PT-symmetric to PT-broken phase where the eigenvalues are complex conjugates, which leads to interesting phenomena^{20–24} like loss-induced single-mode lasing^{5,6,25}, unidirectional waveguiding of chiral modes^{7–9}, non-trivial topology^{26,27} and Brillouin lasers with bistable memory²⁸. The understanding of EPs is crucial for dispersion engineering and polarization-based control in exciton-polaritons, where a PT-symmetric system is yet to be realized due to the coupled exciton and photonic modes both being inherently lossy.

In this work, we embed an optically biaxial semiconductor with linearly polarized excitons in a microcavity, creating anisotropic exciton-polaritons where the coupling strength and detuning is determined by the relative orientation of the polarized incident light and the crystal. Thus, we find a robust way to realize exceptional points, and even tune their location in the dispersion of the polarized polariton modes for potential applications like in the making of a polaritonic PT-symmetry based laser. Crucially, the embedded material, multilayer Rhenium disulphide^{29,30} (ReS₂) offers a large number of Raman modes due to its low symmetry³¹, which when pumped resonantly at an EP, can provide the gain mechanism required to realize a PT-symmetric system from a purely lossy photonic cavity. This offers the potential system to realize a zero threshold polariton Raman laser (to appear soon).

The microcavity structure inherits optical biaxiality from the optically active layer of ReS₂, which lifts the degeneracy between the transverse-electric (TE) or s-polarized and transverse-magnetic (TM) or p-polarized cavity modes. We observe four polariton branches in angle-

resolved reflectance measurements, resulting from the coupling between the two primary exciton species in ReS₂ and the anisotropic cavity's TE and TM modes. We find that by rotating the polarization of incident white light, the interaction strength between the two exciton and cavity modes can be changed from the strong to weak light-matter coupling regime. Modelling this with a 4x4 Hamiltonian yields a peak coupling strength of ~ 18 meV. The ability to tune coupling strength, as well as energy detuning with incident angle due to the cavity modes' finite dispersion, allows for the realization of four sets of EP pairs in this system. The orientation of the crystal with respect to the laboratory frame also tunes the polariton dispersion due to the change in the refractive index corresponding to the TE and TM cavity modes. For specific orientations of the sample, we discover Voigt EPs where the polariton branches corresponding to different polarizations coalesce. This shows the ReS₂ microcavity system can be a viable platform for observing EP-related phenomena like loss-controlled zero-threshold lasing, non-trivial topology, and PT-symmetry breaking.

Results

Anisotropic optical microcavity

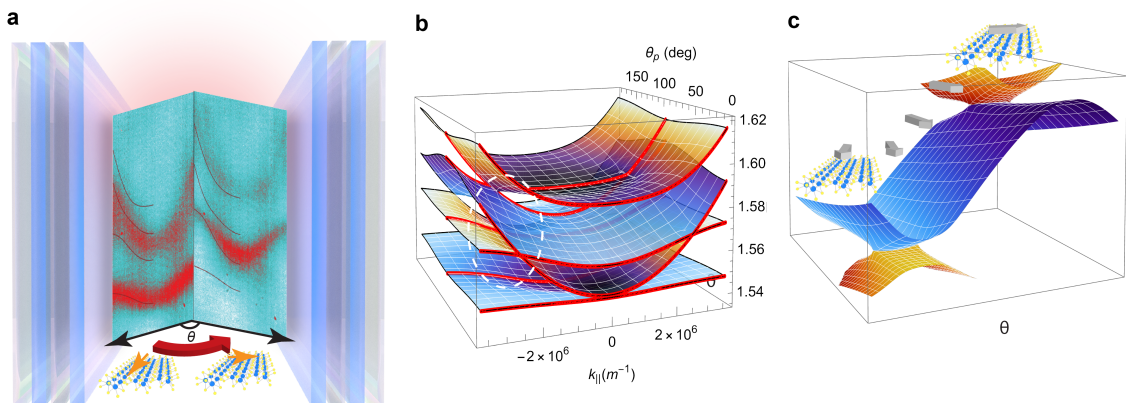


Fig 1. a. Schematic of ReS₂ embedded in a microcavity, showing the incident-angle resolved reflectance for two different incident light polarizations which reveal the X₁ and X₂ polariton dispersions. X₁ and X₂ alignments are marked with orange arrows, making approximately -10° and 80° with the b-axis respectively. **b.** Three-dimensional plot of the polariton dispersions, as a function of in-plane momentum and polarization angle θ . The red curves mark the polariton branches for $\theta = 0^\circ$ and 90° . **c.** Zoomed-in view of the dispersion region

marked with dotted white ellipse in **(b)** clearly showing the exceptional points that are probed by changing θ .

Fig 1(a) shows a schematic of the microcavity used in this work, where the optically active 10 nm ReS₂ multilayer is embedded between two distributed Bragg reflectors (DBRs). The bottom mirror consists of 10 pairs of SiO₂/Ta₂O₅, while the top mirror has 8 pairs to allow for preferential out-coupling of light from the cavity in the direction of collection. The center wavelength λ_{DBR} of the DBRs has a gradient across the substrate due to varying deposition rate of the dielectrics. The ReS₂ sample in this case is embedded where λ_{DBR} is approximately 735 nm. ReS₂ is known to harbor two exciton species, X₁ and X₂, with specific angles with respect to the crystallographic b-axis. Due to the optical biaxiality of ReS₂, light propagating along the z-direction will encounter two different refractive indices based on the electric field polarization direction. This leads to two separate cavity modes, based on different refractive indices n_c corresponding to the two different principal optical axes for propagation along the z-direction. To a very good approximation, their dispersion can be written as:

$$\hbar\omega(k) = E_{cav} + \frac{\hbar^2 k^2}{2m_{ph}}; E_{cav} = \frac{\hbar c \pi}{n_c L_c}, m_{ph} = \frac{\hbar \pi n_c}{c L_c}$$

The cavity length L_c in this expression as well as the refractive index n_c needs to be modified for the cavity with an anisotropic optical medium embedded inside. L_c in this case is $\frac{\lambda_{cav}}{2n_{SiO_2}} + L_{ReS_2}$, while n_c can be taken to be the length-weighted average, $\frac{n_{SiO_2} L_{SiO_2} + n_{ReS_2} L_{ReS_2}}{L_{SiO_2} + L_{ReS_2}}$, with n_{ReS_2} being different for TE and TM polarizations. In addition, since E_{cav} is detuned from the central energy of the DBRs forming the microcavity due to the presence of ReS₂, TE-TM splitting must also be considered. In this case, where $E_{cav} > E_{DBR}$, the TM mode will show larger dispersion than TE at higher incident angles^{32,33}.

Polarization angle tuned cavity polariton dispersion

To perform incident polarization-resolved reflectance, white light from a broadband halogen source is first linearly polarized and sent through a half-wave plate (HWP), which can be rotated to change the angle of incident linear polarization θ . As shown in Supplementary Figure S1, rotating θ changes the relative amplitudes of the TE and TM electric field incident on the sample. The experimental setup is arranged such that the spectrometer detects the TM mode reflectance when $\theta = 0^\circ$. The in-plane components of the TE and TM mode are thus $E\sin\theta$ and $E\cos\theta\cos\phi$, where ϕ is the angle of incidence. Since a 60x objective lens with 0.7 NA is used to focus the beam onto the sample, ϕ ranges from 0 to 45° . The back focal plane of the objective lens is imaged to obtain a one-shot in-plane momentum vs energy dispersion of the reflected light. Vignetting due to the limited aperture of the tube lens collecting the reflected light, causes the effective observation of dispersion up to reflectance angle $\phi \sim 24^\circ$.

The results of the measurements are plotted in Supplementary Figure S2, where we find clear evidence of strong light-matter coupling, with the two exciton resonances X_1 and X_2 coupling with the two anisotropic cavity modes to form four polariton modes. All measurements were taken at 4K, with the sample mounted in a closed-cycle Helium cryostat. As θ is changed, up to four resolvable polariton branches can be seen in the reflectance. For each of the values of $\theta = 60^\circ$ and 140° , the absorption from a different pair of branches is maximized. This is due to the linearly polarized excitons' oscillator strengths being maximum in those directions, with 60° corresponding to X_1 and 140° to X_2 . These angles, denoted as θ_1 and θ_2 , are determined by the sample orientation in the lab frame.

The observed polariton dispersions can be modelled using a four-body coupled oscillator Hamiltonian, expressed here in the basis of creation and annihilation operators, C_i^\dagger denoting the photon creation operator and X_j^\dagger the exciton creation operator:

$$H = C_i C_i^\dagger \hbar \tilde{\omega}_i + X_j X_j^\dagger \hbar \tilde{\omega}_j + [C_i X_j^\dagger + C_i^\dagger X_j] v_j \hat{e}_i \cdot \hat{d}_j \dots (1)$$

Summation over the indices i and j is implied. \hat{e}_i denotes the unit vector along the two electric field modes, with $i=s$ (p) for TE mode (TM mode), and \hat{d}_j indicates the unit vector along which the absorption from each of the linearly polarized exciton species is maximum, with $j=1,2$ for X_1 and X_2 exciton species respectively. $\tilde{\omega}_i$ and $\tilde{\omega}_j$ denote the complex angular frequencies of the bare cavity mode and excitons respectively, with their imaginary part being the half-width half maximum linewidths. The inclusion of these imaginary parts, or losses, in the Hamiltonian renders it non-Hermitian.

Since the two exciton species are at $\sim 80^\circ$ to each other rather than completely orthogonal, the TE and TM modes of the electric field in the cavity couple to both the species of excitons. This is reflected in the off-diagonal terms of the Hamiltonian matrix, $g_{ij} = v_j \hat{e}_i \cdot \hat{d}_j$, which represent the various coupling strengths. All the four types of coupling in this system have an explicit dependence on θ (e.g., for the coupling of X_1 with TM mode, $g_{p1} = v_1 \hat{e}_p \cdot \hat{d}_1 = v_1 \cos\theta \cos\phi \cos\theta_1$ and so on).

The model is fitted with the observed polariton dispersions at $\theta = \theta_1$ and θ_2 , yielding the coupling strength amplitudes v_1 and v_2 to be 14.5 and 18.6 meV respectively. The dispersion fits are shown as white curves superimposed on the experimental reflectance in Fig S2. The coupling strengths g_{ij} are tuned from their maximum values of (e.g., $v_1 \cos\theta_1$ for g_{p1}) to zero by changing θ , which results in a transition from strong to weak light-matter coupling between the four oscillator modes in this system. Further, the energy detuning between the

uncoupled modes changes with in-plane momentum $k_{||}$ or incidence angle ϕ because of the inherent dispersion of the cavity modes. Being able to explore this parameter space offers the possibility of realizing EPs in this system.

Fig 1(b) shows a 3D plot of the real eigenenergy surfaces for the four-body coupled oscillator system, in the parameter space of θ and $k_{||}$, using parameter values extracted from fitting as mentioned previously. As expected from the model, near $\theta = 90^\circ$ the TM mode electric field component and therefore the corresponding coupling strength $g_{p2} \propto \cos\theta$ approaches zero, falling below the threshold for strong coupling. At $k_{||} = \pm 2.2 \mu\text{m}^{-1}$ where the TM mode and X2 exciton have zero energy detuning, the anti-crossing is removed, and a pair of EPs are realized as θ is tuned to around 90° . These are marked as blue dots on the energy surfaces in Fig 1(c). The corresponding position of the EPs in the experimental reflectance data is shown in Fig S3(a), by taking the cross-section at $k_{||} = \pm 2.2 \mu\text{m}^{-1}$ for the reflectance data taken for θ varying from 0° to 360° .

Similarly, the TE mode-related component $g_{s2} \propto \sin\theta$ approaches zero at $\theta = 0^\circ$ and 180° . At $k_{||} = \pm 2.6 \mu\text{m}^{-1}$, the TM mode and X2 energy detuning is such that another pair of EPs is created. These are marked as red dots in Fig 1(c) and indicated in the experimental cross-section data in Fig S3(b) with a dotted circle. The reduced absorption by the polariton branches near the EPs make the coalescing difficult to observe in the experimental reflectance, but their presence can be surmised from the change in coupling strengths in the Hamiltonian, and extrapolation of the experimental data.

Orientation-based realization of Voigt Exceptional Points

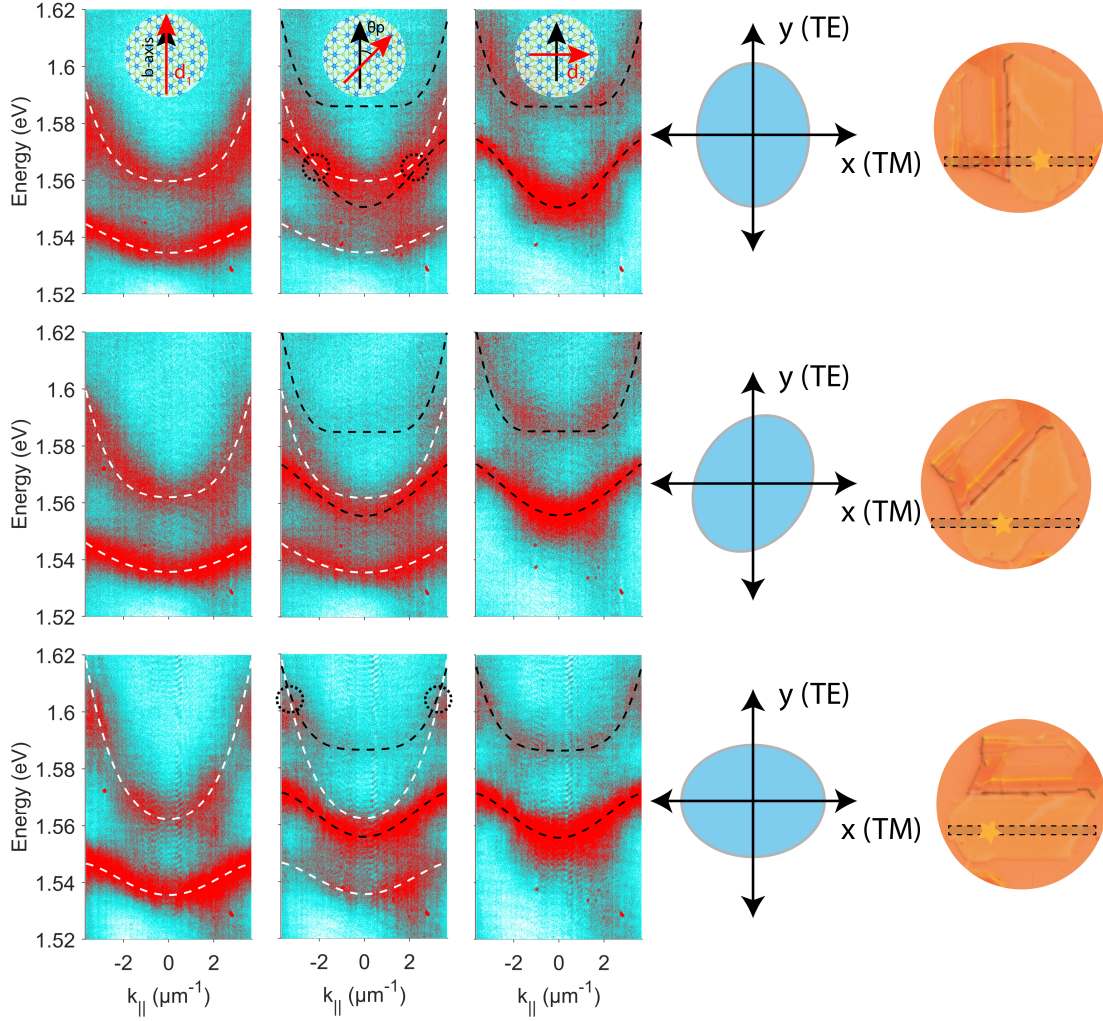


Fig 2. Orientation dependent polariton dispersion and realization of Voigt EPs. First three columns show the incidence angle resolved reflectance for three different incident beam polarizations, along \hat{a}_1 , intermediate, and \hat{a}_2 , as indicated by the insets in the topmost row. The intermediate case reveals the Voigt EPs where the polariton modes coalesce (marked by black dotted circles). Last two columns represent the refractive index ellipsoid and the sample orientation with respect to the laboratory frame corresponding to the reflectance data shown in the first three columns. The projection of the spectrometer slit is marked as a black dotted rectangle on the sample image.

The orientation of the sample b-axis in the laboratory frame is crucial in deciding the occurrence and nature of EPs in the system. Essentially θ_1 and θ_2 , the orientations of the excitons with respect to the TM cavity mode which is aligned along the laboratory x-axis, are

decided by the orientation of the mounted sample. In addition, the dispersion of the TE and TM modes are changed since the refractive index corresponding to these polarization directions is also changed with orientation. In the previous section examining polarization-tuned coupling, θ_1 was fixed at 60° . In Fig 2, the angle-resolved reflectance data for sample orientations $\theta_1 = 0^\circ, 45^\circ$ and 90° are shown for when the incident polarization is kept along \widehat{d}_1 , an intermediate direction, and \widehat{d}_2 . For polarization along \widehat{d}_1 , only two polariton branches are ‘probed’ or visible as absorption lines. We denote the upper and lower polariton associated with the \widehat{d}_1 direction as U1 and L1 respectively. Similarly, for incident polarization along \widehat{d}_2 we observe two polariton branches corresponding to X_2 , thus denoted U2 and L2. In the intermediate incident polarization state, all four branches are observed, and we find for specific orientations the polariton branches coalesce at specific values of in-plane momentum, or incidence angle. These points represent a class of EPs known as Voigt points. In this system, this is achieved when the difference in energy between TE and TM modes at zero incidence angle caused by birefringence is compensated by the TE-TM splitting at higher angles. For $\theta_1 = 0^\circ$, we find a pair of Voigt EPs at ~ 1.56 eV and $k_{\parallel} = 1.8 \mu\text{m}^{-1}$ where the branches U1 and L2 coalesce. For $\theta_1 = 90^\circ$, Voigt EPs are formed when U1 and U2 coalesce, at ~ 1.6 eV and $k_{\parallel} = 3.5 \mu\text{m}^{-1}$.

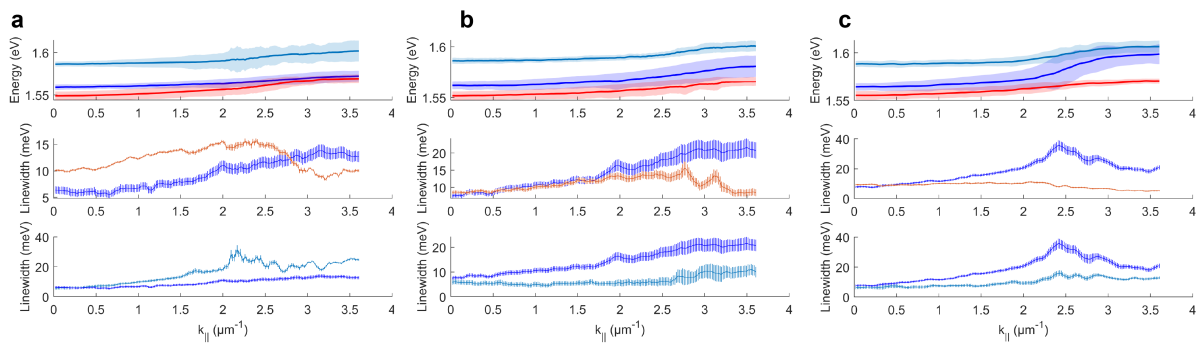


Fig 3. Extracted energies and linewidths (FWHM) of polariton branches for different sample orientations. The topmost plot shows the extracted energy dispersions of L2 (red), U1 (blue) and U2 (light blue) for sample orientation **a.** $\theta_1 = 0^\circ$, **b.** $\theta_1 = 45^\circ$, **c.** $\theta_1 = 90^\circ$, with the color spread denoting the linewidth. The corresponding polariton linewidths are plotted with the same colour in the middle and bottom panels, revealing crossing and anti-crossings if any. The error bars represent 95%

confidence intervals of the fitted value. For $\theta_1 = 0^\circ$, we see a clear crossing of the linewidths of U1 and L2 near the EP where the real eigenvalues also nearly coalesce.

To probe the complex eigenvalues of the polaritons, we carefully extract the position and linewidths of the polariton branches for incident polarization along \widehat{d}_1 and \widehat{d}_2 directions, by fitting the absorption dips with Lorentzian functions. The results are shown in Fig 3. In Fig 3(a) corresponding to sample orientation $\theta_1 = 0^\circ$, we find that the real values of U1 and L2 branches coalesce, and in the same $k_{||}$ range the linewidths show a crossing, clearly revealing an EP where the complex eigenvalue of both modes have coalesced. In Fig 3(b) where $\theta_1 = 45^\circ$, no EPs are observed, with the polariton branches showing level repulsion characteristic of strong coupling while the linewidths also don't show any crossing. For $\theta_1 = 45^\circ$ in Fig 3(c) we find that while the real values of U1 and U2 coalesce at a high $k_{||}$, we see an anti-crossing in the linewidths. This indicates that the critical condition for realizing an EP is not achieved in this case, and the coupling strength is such that the system is in a PT-broken phase. The bottom panel shows the linewidth of U1 and U2 are approaching each other, so a Voigt point may form at a higher $k_{||}$ than which can be probed with our current setup. This possibility is explored by using our 4x4 Hamiltonian model to simulate the polariton dispersions.

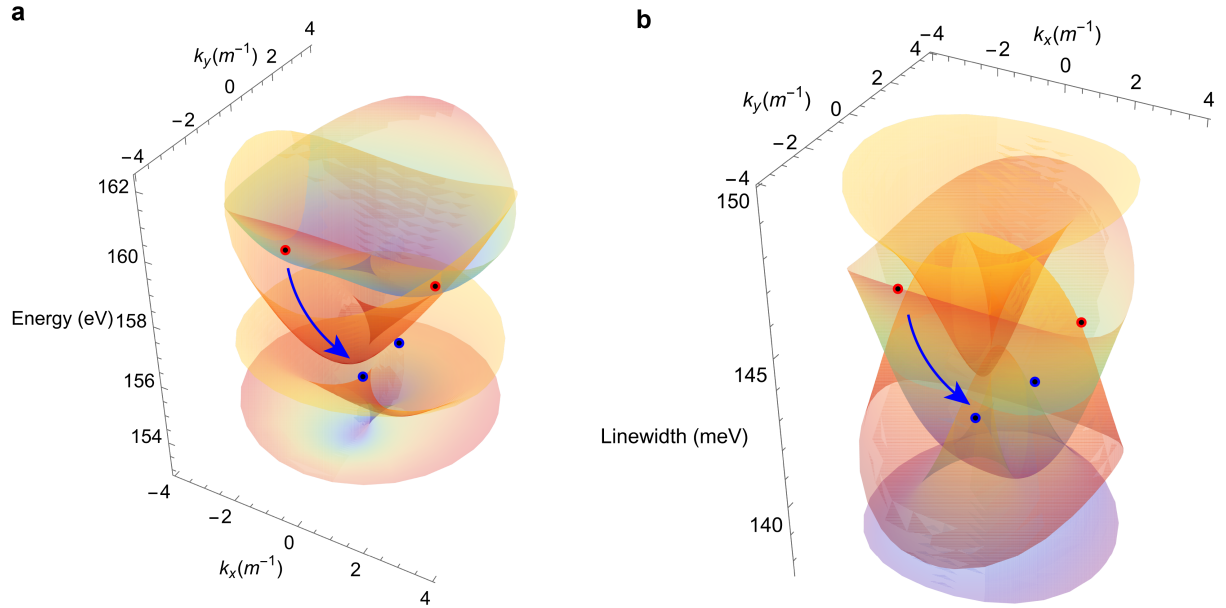


Fig 4. a, b Real and imaginary parts of the eigenenergy of the 4x4 Hamiltonian, as a function of k_x and k_y . Two sets of exceptional points (EPs) are marked with red and blue dots where the eigenvalues coalesce to form Voigt EPs. Blue arrow indicates a trajectory to adiabatically tune the system from one EP to another by varying k_y .

A co-ordinate transformation of the 4x4 Hamiltonian given in Eqn (1) by fixing the value of θ and considering only the change in θ_1 allows us to go from $k_{||} - \theta$ space to $k_x - k_y$ space which reveals the sample orientation or θ_1 dependent dispersion of the polaritons, shown in Fig 4. In this case, the refractive index corresponding to the TE or TM mode is θ_1 dependent, which we model as $n_{c1} = \sqrt{(n_{cx} \cos \theta_1)^2 + (n_{cy} \sin \theta_1)^2}$ and $n_{c2} = \sqrt{(n_{cx} \sin \theta_1)^2 + (n_{cy} \cos \theta_1)^2}$ which represents the index ellipsoid of the optically active biaxial ReS₂ for propagation in the z-direction. n_{cx} and n_{cy} are extracted first by fitting the polariton branches for the cases when $\theta_1 = 0^\circ$ and 90° respectively. In Fig 4(a) we find two sets of Voigt EPs revealed, as found in our experimental results, one set between U1 and L2, and one set between U1 and U2. Fig 4(b) shows the corresponding linewidths that also show crossing near the Voigt points. On changing the parameter θ_1 or $k_{||}$, the state of the system can be quasi-adiabatically tuned and encircled around an EP, which will cause a ‘flipping’ of

the state where the real value stays the same while the imaginary part changes after one encirclement.

Prescription for realizing a PT-symmetric system

The uncoupled cavity and exciton modes in Eqn (1) have an inherent lifetime after which they decay, signified by a negative sign of their complex energy values. This property is inherited by the polariton modes which are also lossy and have a finite lifetime. To make the system PT-symmetric, a mechanism to introduce gain in to one of the modes is required. If a low-symmetry material with a large number of Raman modes is embedded in the cavity, then it becomes possible to pump the cavity resonantly at one polariton branch, and ensure one of the Raman Stokes lines coincides with another polariton branch at a lower energy. By changing the pump power, it is possible to tune the gain or loss of the resonant polariton-Raman mode state and thus achieve PT-symmetry. This manifests as lasing associated with the Raman mode resonant with a polariton branch. Further, the EPs in this system as well as the polarized cavity modes can be exploited to achieve thresholdless lasing. By pumping at an EP, both polarization states are excited, while only the Raman polarization state that is resonant with a cavity mode is enhanced and starts lasing. Since only one mode participates in the lasing process (instead of all polarizations in an isotropic microcavity), the result is truly thresholdless lasing. The experimental realization of this is discussed in detail in our other work (Manuscript to appear soon).

Discussion

In summary, linearly polarized exciton-polaritons in ReS₂ offer an excellent platform to observe non-Hermitian phenomena due to the direct control over coupling strength. While incident polarization resolved reflectance offers a clear window into the presence of EPs in

the polariton dispersion, richer physics can be found in the photoluminescence from the polaritons near the EPs. However, due to the quasi-indirect bandgap of ReS₂, the PL quantum yield of ReS₂ is poor and the signal near the EPs, which occur at the upper and middle polariton branches, is too weak to be observed. The low symmetry structure of ReS₂ offers another route to explore the effect of EPs, due to the presence of several polarized Raman modes.

Acknowledgements:

This work has been supported by funding from the Science and Engineering Research Board (CRG/2018/002845, CRG/2021/000811); Ministry of Education (MoE/STARS- 1/647); Council of Scientific and Industrial Research, India (09/081(1352)/2019-EMR-I); Department of Science and Technology, Ministry of Science and Technology, India (IF180046) and Indian Institute of Technology Kharagpur.

Author contributions:

SD conceptualized the project. DC, AD, KG, ARC and SD contributed in the sample fabrication. DC, AD, PD and SD formulated the experiments, performed data analysis, and developed the theory. DC, AD, performed all optical measurements. DC, AD, and SD drafted the paper, and all authors contributed to reviewing and editing the final draft. SD supervised the project.

References

1. Feng, L., El-Ganainy, R. & Ge, L. Non-Hermitian photonics based on parity–time symmetry. *Nat. Photonics* **11**, 752–762 (2017).
2. El-Ganainy, R. *et al.* Non-Hermitian physics and PT symmetry. *Nat. Phys.* **14**, 11–19 (2018).
3. Özdemir, Ş. K., Rotter, S., Nori, F. & Yang, L. Parity–time symmetry and exceptional points in photonics. *Nat. Mater.* **18**, 783–798 (2019).
4. Miri, M.-A. & Alù, A. Exceptional points in optics and photonics. *Science* **363**, eaar7709 (2019).
5. Liertzer, M. *et al.* Pump-Induced Exceptional Points in Lasers. *Phys. Rev. Lett.* **108**, 173901 (2012).
6. Peng, B. *et al.* Loss-induced suppression and revival of lasing. *Science* **346**, 328–332 (2014).
7. Peng, B. *et al.* Chiral modes and directional lasing at exceptional points. *Proc. Natl. Acad. Sci.* **113**, 6845–6850 (2016).

8. Gao, T. *et al.* Chiral Modes at Exceptional Points in Exciton-Polariton Quantum Fluids. *Phys. Rev. Lett.* **120**, 065301 (2018).
9. Nasari, H. *et al.* Observation of chiral state transfer without encircling an exceptional point. *Nature* **605**, 256–261 (2022).
10. Gao, T. *et al.* Observation of non-Hermitian degeneracies in a chaotic exciton-polariton billiard. *Nature* **526**, 554–558 (2015).
11. Gao, W., Li, X., Bamba, M. & Kono, J. Continuous transition between weak and ultrastrong coupling through exceptional points in carbon nanotube microcavity exciton–polaritons. *Nat. Photonics* **12**, 362–367 (2018).
12. Chakrabarty, D. *et al.* Interfacial anisotropic exciton-polariton manifolds in ReS₂. *Optica* **8**, 1488–1494 (2021).
13. Su, R. *et al.* Direct measurement of a non-Hermitian topological invariant in a hybrid light-matter system. *Sci. Adv.* (2021) doi:10.1126/sciadv.abj8905.
14. Khurgin, J. B. Exceptional points in polaritonic cavities and subthreshold Fabry–Perot lasers. *Optica* **7**, 1015–1023 (2020).
15. Richter, S. *et al.* Exceptional points in anisotropic planar microcavities. *Phys. Rev. A* **95**, 023836 (2017).
16. Bender, C. M. & Boettcher, S. Real Spectra in Non-Hermitian Hamiltonians Having $\mathcal{P}\mathcal{T}$ Symmetry. *Phys. Rev. Lett.* **80**, 5243–5246 (1998).
17. Heiss, W. D. The physics of exceptional points. *J. Phys. Math. Theor.* **45**, 444016 (2012).
18. Berry, M. V. Physics of Nonhermitian Degeneracies. *Czechoslov. J. Phys.* **54**, 1039–1047 (2004).
19. Rüter, C. E. *et al.* Observation of parity–time symmetry in optics. *Nat. Phys.* **6**, 192–195 (2010).
20. Ren, J. *et al.* Unidirectional light emission in PT-symmetric microring lasers. *Opt. Express* **26**, 27153–27160 (2018).
21. Doppler, J. *et al.* Dynamically encircling an exceptional point for asymmetric mode switching. *Nature* **537**, 76–79 (2016).
22. Peng, B. *et al.* Parity–time-symmetric whispering-gallery microcavities. *Nat. Phys.* **10**, 394–398 (2014).
23. Chen, W., Kaya Özdemir, Ş., Zhao, G., Wiersig, J. & Yang, L. Exceptional points enhance sensing in an optical microcavity. *Nature* **548**, 192–196 (2017).
24. Zhou, H. *et al.* Observation of bulk Fermi arc and polarization half charge from paired exceptional points. *Science* **359**, 1009–1012 (2018).
25. Hodaei, H., Miri, M.-A., Heinrich, M., Christodoulides, D. N. & Khajavikhan, M. Parity-time-symmetric microring lasers. *Science* **346**, 975–978 (2014).
26. Bergholtz, E. J., Budich, J. C. & Kunst, F. K. Exceptional topology of non-Hermitian systems. *Rev. Mod. Phys.* **93**, 015005 (2021).
27. Yao, S. & Wang, Z. Edge States and Topological Invariants of Non-Hermitian Systems. *Phys. Rev. Lett.* **121**, 086803 (2018).

28. Chen, Y. *et al.* Exceptional points with memory in a microcavity Brillouin laser. *Optica* **9**, 971–979 (2022).
29. Aslan, O. B., Chenet, D. A., van der Zande, A. M., Hone, J. C. & Heinz, T. F. Linearly Polarized Excitons in Single- and Few-Layer ReS₂ Crystals. *ACS Photonics* **3**, 96–101 (2016).
30. Dhara, A. *et al.* Additional excitonic features and momentum-dark states in ReS₂. *Phys. Rev. B* **102**, 161404 (2020).
31. McCreary, A. *et al.* Intricate Resonant Raman Response in Anisotropic ReS₂. *Nano Lett.* **17**, 5897–5907 (2017).
32. Panzarini, G. *et al.* Cavity-polariton dispersion and polarization splitting in single and coupled semiconductor microcavities. *Phys. Solid State* **41**, 1223–1238 (1999).
33. Kavokin, A. V., Baumberg, J., Malpuech, G. & Laussy, F. P. *Microcavities*. (Oxford University Press, 2017).
34. Balili, R., Hartwell, V., Snoke, D., Pfeiffer, L. & West, K. Bose-Einstein Condensation of Microcavity Polaritons in a Trap. *Science* **316**, 1007–1010 (2007).
35. Deng, H., Haug, H. & Yamamoto, Y. Exciton-polariton Bose-Einstein condensation. *Rev. Mod. Phys.* **82**, 1489–1537 (2010).
36. Schneider, C., Glazov, M. M., Korn, T., Höfling, S. & Urbaszek, B. Two-dimensional semiconductors in the regime of strong light-matter coupling. *Nat. Commun.* **9**, 2695 (2018).

Supplementary Materials

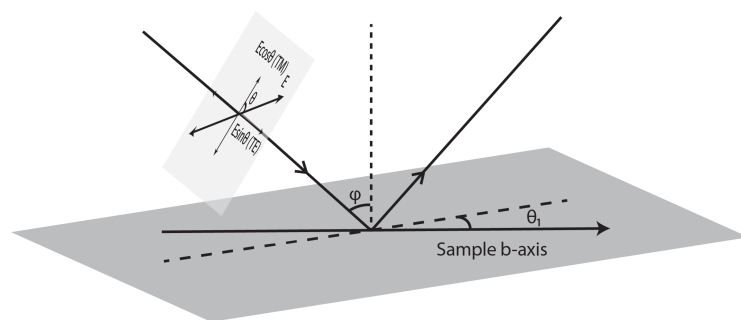


Fig S1. Ray diagram showing how rotation of polarization angle changes the in-plane TE and TM components of incident light for the reflectance setup.

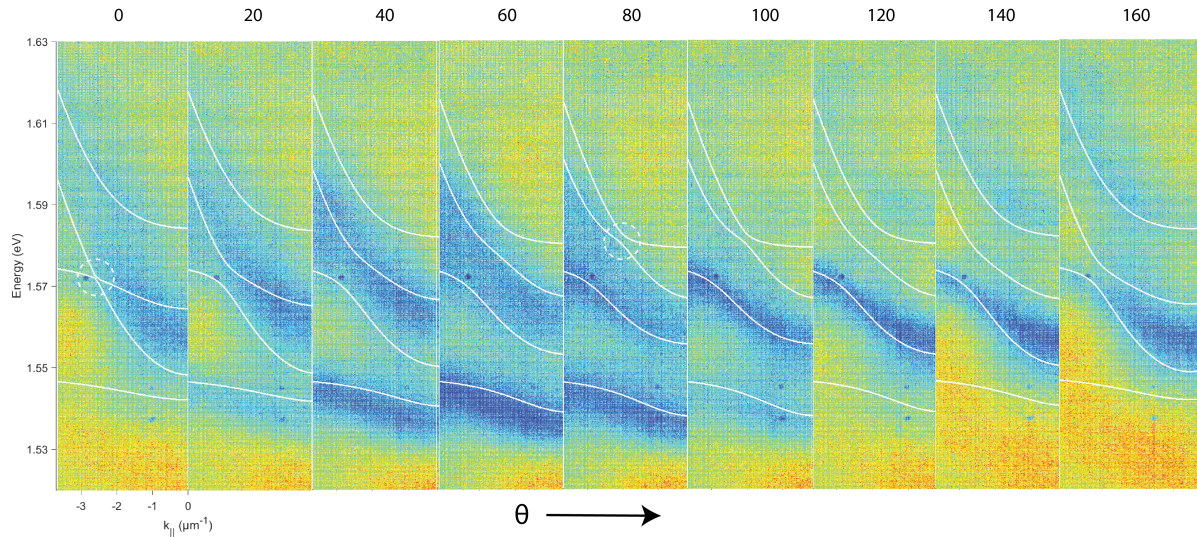


Fig S2. Polarization angle (θ) dependent, angle-resolved reflectance for 10nm ReS₂ in microcavity. White lines mark the polariton dispersions as obtained from a 4x4 coupled oscillator model.

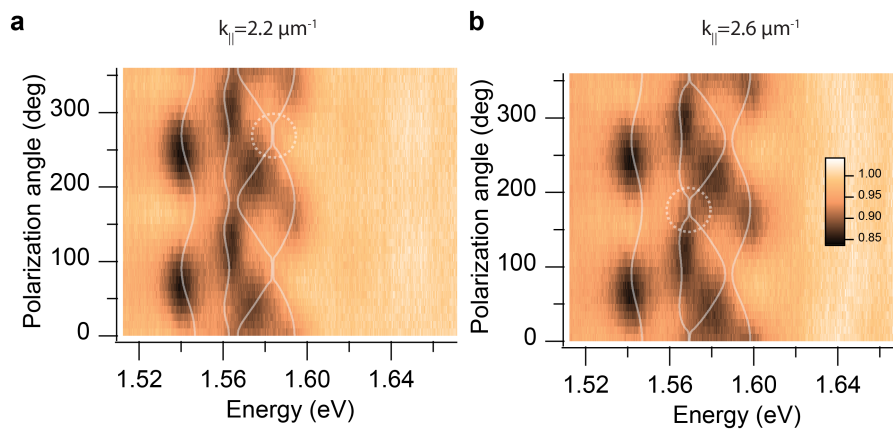


Fig S3. a, b. Experimental reflectance as a function of θ , for fixed k_{\parallel} corresponding to where energy detuning with X2 is zero for TM and TE cavity mode respectively. White translucent curves show the corresponding cross sections of the 3-D eigenenergy surfaces plotted in Fig 1b.

Supplementary Note 1

Cavity exciton-polaritons, which are hybrid light-matter quasiparticles formed by the coupling of excitons with photons inside high-quality optical resonators^{34–36}, offer an ideal

platform to observe non-Hermitian physics due to the inherent losses in the system. The Hamiltonian of a cavity polariton is a 2x2 coupled oscillator matrix:

$$\begin{pmatrix} E_{cav} & g \\ g & E_{ex} \end{pmatrix}$$

Where typically E_{cav} and E_{ex} , the cavity and exciton energies, are complex quantities carrying information about the cavity photon and exciton lifetimes. To probe EPs present in the eigenenergy manifold, the system should have the ability to realize different values of energy detuning ($\Delta = E_{cav} - E_{ex}$) and coupling strength (g). For $\Delta = 0$ and $g = \sqrt{(\Gamma_{cav} - \Gamma_{ex})/2}$, where Γ are the imaginary, dissipative parts of E_{cav} and E_{ex} , the eigenenergies of the polariton modes will coalesce and give rise to an EP.